Journal Materials Chemistry B

ARTICLE

Facile Synthesis of β-Lactoglobulin Capped Ag_2S Quantum Dots for *In Vivo* Imaging in the Second Near-Infrared Biological Window

Received 00th January 20xx,
Accepted 00th January 20xx

DOI: 10.1039/x0xx00000x

www.rsc.org/

Jun Chen,[a§] Yifei Kong,[b§] Yan Wo,[c,d]* Hongwei Fang,[e] Yunxia Li,[a]* Tao Zhang,[f] Yu Dong,[a] , Yunsheng Ge,[a] Ziying Wu,[a] Dejian Zhou[b]* and Shiyi Chen[a]*

Effective *in vivo* fluorescence imaging for cancer screening and diagnostics requires bright and biocompatible fluorophores whose emission can effectively penetrate biological tissues. Recent studies have confirmed that the second near-infrared window (NIR-II, 1,000-1,400 nm) is the most sensitive spectral range for *in vivo* imaging due to ultralow tissue absorption and autofluorescence. We report herein a facile synthesis of Ag_2S quantum dots (QDs) that emits at ~1100 nm using β-lactoglobulin (β-LG) as biological template. The β-LG protein coating improves water-solubility, faciliates rapid biodistribution and reduces *in vivo* toxicity of the QDs. Compared to other currently used NIR emitters, β-LG capped Ag_2S QDs exhibit superior photostablity and biocompatibility, making them a promising probe for *in vivo* NIR-II imaging.

1. Introduction

Compared to other available imaging modalities such as magnetic resonance imaging (MRI), positron emission tomography (PET) and computed tomography (CT), fluorescence based optical imaging is attractive due to their advantages of fast image acquisition, higher spatial resolution and absence of ionizing radiation.[1-3] In this respect, the fluorophores emitting in the second near infrared biological window (NIR-II, 1,000-1,400 nm) is particularly advantageous over those emitting at the visible (400-650 nm) or first near-infrared (NIR-I, 650-900 nm) regions because of the greatly reduced light absorption and photon scattering together with negligible tissue autofluorescence[4, 5]. As a result, NIR-II fluorescence imaging can allow deep penetration into biological tissues with excellent imaging fidelity, sensitivity and resolution.[5-7] Over the past few years, considerable efforts have been devoted to develop high-quality NIR-II emitters including single-walled carbon nanotubes (SWNTs),[8-10] quantum dots (QDs), [11-17] rare-earth-doped nanoparticles (NPs),[18-20] and polymeric fluorophores.[21, 22] Among them, the no toxic heavy metal-containing Ag_2S QDs have become one of the most intensively studied NIR-II emitters.[23] Recently, Wang and coworkers have made substantial progress in the preparation and exploitation of NIR-II-emitting Ag_2S QDs for biomedical applications, including blood system visualization[24], tumour targeting chemotherapy [25] and *in vivo* stem cell distribution tracking.[26, 27] Moreover, a long-term *in vivo* study on animal models verified the ultralow accumulation of Ag_2S QDs in vital organs[28]. Despite such progress, the current methods for synthesizing Ag_2S QDs are suffering from the requirement of high temperature and nonpolar organic solvents that lead to the hydrophobic QDs. It is well known that the biology-related applications request a high solubility of QDs in aqueous solution; thus, a phase transfer at post-synthesis is needed as well as achieved through amphiphilic molecule encapsulation and/or surface modification with hydrophilic ligands. Such a step can sometimes adversely affect the optical properties of QDs and compromise the *in vivo* application efficiency.[29-32] On this point, the development of aqueous syntheses for biocompatible, water-soluble and NIR-II-emitting Ag_2S QDs is valuable.

Recently, the use of biomolecules (*e.g.*, peptides and proteins) as soft templates for preparing NIR-II Ag_2S QDs in the aqueous phase has been reported [33, 34]. However, their poor quantum yields (QYs) hinder their further biological applications (Table.S1, ESI†), especially *in vivo* imaging. β-lactoglobulin (β-LG), a main component of whey proteins in bovine milk, is a small protein containing 162 amino acids (MW: ~18.4 kDa).[35] It has been widely used as a carrier for bioactive molecules without covalently bonding.[36, 37] Compare to other proteins, β-LG has a high structural and proteolytic stability at acidic pHs but can readily lose its quaternary and tertiary structures at basic pHs.[38, 39] This interesting properties allow the β -LG encapsulated drugs to retain a high stability in the acidic stomach whereas induce their release in the small intestine's basic environment.[35] Upon binding to hydrophobic retinoids or vitamin D, the β-LG conjugates can directly penetrate cell membrane and enter cytosol without being entrapped in the endosomal-lysosomal system.[40, 41] Inspired by

[a] *Department of Orthopedic Sports Medicine, Huashan Hospital, Fudan University, Shanghai 200040, China.*
E-mail: liyunxia912@aliyun.com (Y.L.), cshiyi@163.com (S.C.); Tel&Fax: (+) 86-021-52888255.
[b] *School of Chemistry and Astbury Structure for Molecular Biology, University of Leeds, Leeds LS2 9JT, UK. E-mail: d.zhou@leeds.ac.uk.*
[c] *Department of Human Anatomy, Histology and Embryology,School of Medicine, Shanghai JiaoTong University, Shanghai 200025,China. E-mail: woyansh@gmail.com.*
[d] *Department of Plastic and Reconstructive Surgery, Shanghai Ninth People's Hospital, School of Medicine, Shanghai JiaoTong University, Shanghai 200011, China.*
[e] *Department of Anesthesiology, The First Affiliated Hospital of Bengbu Medical College, Anhui 233004, China.*
[f] *Department of orthopedics, The second hospital of Fuzhou Affiliated to Xiamen University, Fuzhou 350007, China.*
[§] *These authors are contributed equally.*
†Electronic Supplementary Information (ESI) available . See DOI: 10.1039/x0xx00000x

the attractive properties, we report herein a one-pot aqueous synthesis of NIR-II-emitting Ag_2S QDs using β-LG as the capping/stabilizing agent. The β-LG-encapsulated Ag_2S QDs (β-LG-Ag_2S QDs) disperse well in water and stably emit in the NIR-II region peaking at ~1100 nm. Despite minimal effect on cell growth and proliferation, the β-LG-Ag_2S QDs are considered to be adequately safe for *in vivo* fluorescence imaging.

2. Materials and Methods

2.1 Materials

Silver nitrate (≥ 98.0%), sodium sulfide nonahydrate (≥ 98.0%), sodium hydroxide (≥ 98.0%) and β-lactoglobulin (β-LG, MW: ~18.4 kDa) were purchased from Sigma-Aldrich. 3-(4,5-Dimethylthiazol-2-yl)-2,5-diphenyltetrazolium bromide (MTT), DMEM, FBS, penicillin, streptomycin and trypsin-EDTA were purchased from commercial sources. Ultrapure Millipore water (resistivity: 18.2 mΩ•cm) was used make solutions and buffers. All other reagents were of at least analytical grade and used without further purification.

2.2 Synthesis of Water-Soluble β-LG-Ag_2S QDs

In a typical synthesis, 500 μL of 50 mg mL^{-1} β-LG was mixed with 500 μL of 10 mM $AgNO_3$ under continuous stirring at RT for 5 min. The pH of the solution was then adjusted with 10 μL of 1 M NaOH. Immediately, 300 μL of 10 mM Na_2S was quickly injected into the solution followed by heated at 100 °C for 1 min under microwave irradiation by the microwave system (Discover, CEM of American). The resulting solution was cooled to RT, ultrafiltered using a centrifugal filtering device (Millipore, 10kDa molecular weight cutoff) and then washed three times with 1 × PBS. The obtained Ag_2S QDs suspension was stored in darkness at 4°C for subsequent experiments.

2.3 Characterization

Transmission electron microscopy (TEM), high-angle annular dark-field scanning transmission electron microscopy (HAADF-STEM), selected area electron diffraction (SAED) and energy dispersive X-ray (EDX) analysis were performed in an FEI Tecnai F20 field emission gun TEM/STEM microscope operated at 200 kV and fitted with a Fischione HAADF detector and an 80 mm^2 X-Max Silicon Drift Detector (SDD) (Oxford Instruments) and a Gatan Orius SC600A CCD camera. The hydrodynamic sizes and size distributions of the β-LG-Ag_2S QDs were measured on a Zetasizer NanoSampler instrument (Malvern). Powder XRD patterns were recorded on a Bruker Advance powder X-ray diffractometer *via* Cu Kα radiation (λ=1.5406 Å). UV/visible/NIR spectra were recorded on a LAMBDA 950 UV/Vis/NIR spectrophotometer. NIR-II fluorescence spectra were recorded on an NS1 NanoSpectralyzer® fluorimetric analyzer (Applied NanoFluorescence) under an excitation wavelength of 785 nm. To examine the photoluminescence (PL) stability of the β-LG-Ag_2S QDs, the QDs were firstly incubated in PBS (1 mM, pH 7.0), DMEM and FBS at 4°C. The QDs were then dispersed in various buffers (pH= 5.4, 7.4 and 9.8) at different temperatures, and the QD PL intensities were recorded at different time intervals (0–168 h).

2.4 MTT Assay

The cytotoxicity of the β-LG-Ag_2S QDs to 293T, GES-1 and MC3T3-E1 cells was determined using an MTT cytotoxicity assay. The cells were cultured overnight in 96-well plates (2×10^3 cells per well) to enable cell attachment and then incubated in 200 μL of fresh cell media containing 0, 0.8, 8, and 80 nM β-LG-Ag_2S QDs for 24 h. Cell viabilities were measured using a standard MTT assay kit according to the manufacturer's instructions. The cell viability levels was determined using the following equation:

$$\text{Cell viability \%} = OD_{490nm}\ (\text{sample}) / OD_{490nm}\ (\text{control}) \times 100\%$$

The cell viability of the blank control (healthy cells) was defined as 100%, and the cell viability of the treated cells was expressed as a percentage (%) of the control value.

2.5 Cell Apoptosis and Cell Cycle Assay

Apoptosis and necrosis processes of the 293T, GES-1 and MC3T3-E1 cells induced by exposure to 0, 8, and 80 nM β-LG-Ag_2S QDs for 24 h were measured using an apoptosis and necrosis assay kit according to the manufacturer's instructions. In brief, the 293T, GES-1 and MC3T3-E1 cells were plated onto a six-well plate at a density of 2×10^5 cells per well overnight and then treated with 0, 8, and 80 nM of β-LG-Ag_2S for 24 h. The cells were harvested, washed twice with PBS, resuspended in 500 μL of PBS, and finally incubated in anti-annexin V-Fluorescein isothiocyanate (FITC) and propidium iodide (PI).

2.6 In Vivo Imaging

Four- to six-week-old nude female mice were obtained from the Experimental Animal Center of the Chinese Academy of Sciences in Shanghai, China. The mice were raised in an animal facility under filtered air conditions (22 ± 2°C), fed a standard pellet diet and provided pure water. The study was performed within the Guidelines for the Care and Use of Research Animals. Tumor model animals were generated *via* subcutaneous inoculation (2-3 million cells/100 μL of media) of the human osteosarcoma cell line MNNG/HOS (ATCC NO: CRL-1543TM) using a 1 mL syringe with a 25G needle (2-3 million cells/100 μL of media). Then, a 200-μL aliquot of the β-LG-Ag_2S QDs at a concentration of 80 nM was intravenously injected into the tail vein. At various time points during injection and imaging, the mice were anesthetized with isoflurane. NIR-II fluorescence images were collected using a two-dimensional InGaAs array (Photonic Science) for collecting photons in the NIR-II region. An 808-nm diode laser was used as an excitation light source and filtered by 850- and 1,000-nm short-pass filters. The excitation power density level along the imaging plane was 15 mW cm^{-2}, which is much lower than the safe exposure limit of 329 mW cm^{-2} at 808 nm outlined by the International Commission on Nonionizing Radiation Protection. The emission signals from the animal were filtered through an 1100-nm long-pass filter coupled with an InGaAs camera for NIR-II imaging. These *in vivo* images were further utilized for surface plot analysis using *ImageJ* software (National Institutes of Health, USA).

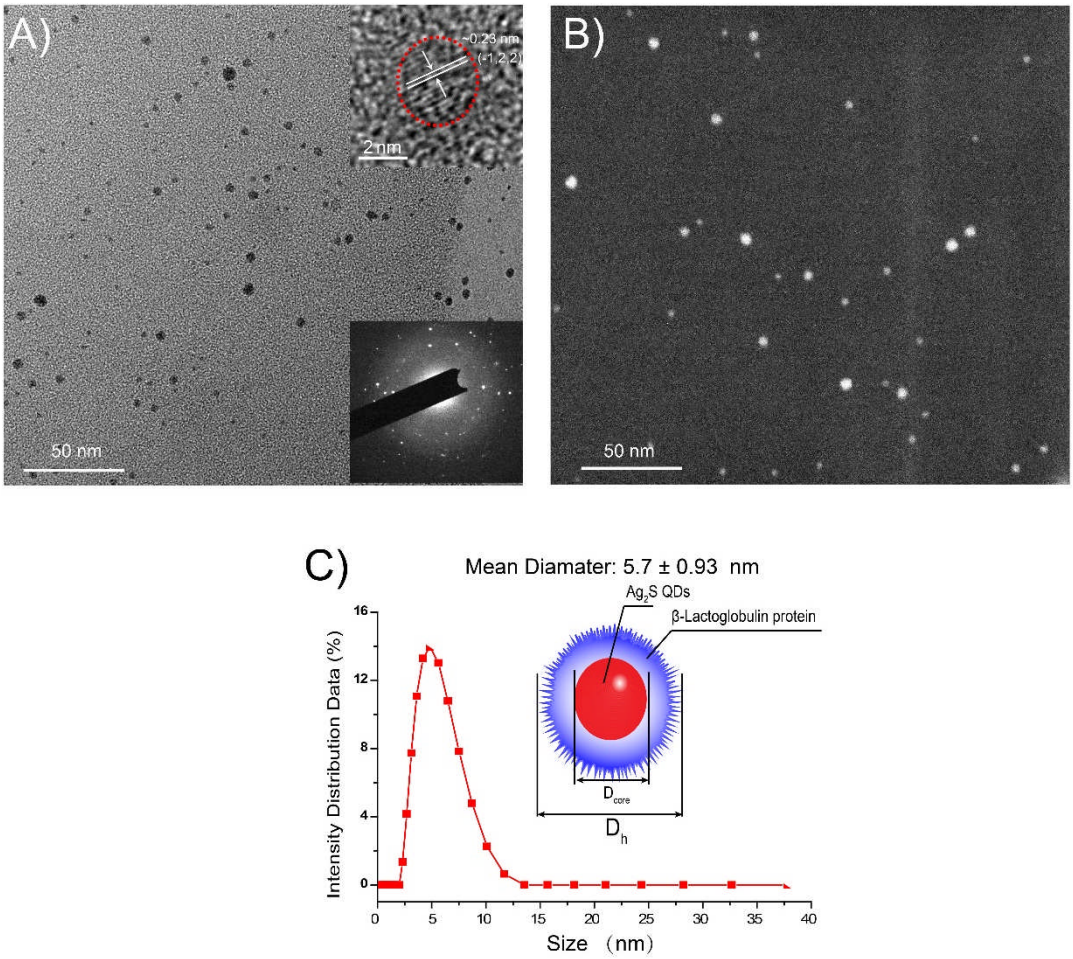

Fig. 1. Morphological and size analysis of β-LG-Ag_2S QDs. (A) TEM image of as-prepared Ag_2S QDs. Upper inset: HR-TEM image of an individual Ag_2S QD denoted by a dotted line; lower inset: corresponding SAED pattern. (B) HAADF-STEM image of the Ag_2S cores. (C) Hydrodynamic diameter of β-LG-Ag_2S QDs in aqueous phase. Inset: schematic illustration of the β-LG-Ag_2S QD hybrid structure.

3. Results and Discussion

3.1. Morphological & Structural Characterization

The morphology of freshly prepared β-LG-Ag_2S QDs were imaged using transmission electron microscopy (TEM). Fig. 1A shows that the quasi-spherical Ag_2S QDs are well dispersed without noticeable aggregation. A high-resolution TEM (HR-TEM) image (Fig. 1A inset) shows an individual Ag_2S particle with a well-resolved lattice plane. Moreover, the crystal structure can be indexed to monoclinic Ag_2S (JCPDS No: 65-2356) according to the X-ray diffraction pattern (Fig. S1, ESI†). An energy dispersive X-ray (EDX) analysis confirms the presence of Ag and S with an atomic ratio (Ag:S) of 1.68:1 (Fig. S2, ESI†). High-angle annular dark-field scanning transmission electron microscopy (HAADF-STEM) allows for precise determination of the QD core size to be 4.3 ± 0.65 nm (Fig. S3, ESI). The overall size of the hybrid structure was further imaged by tapping-mode atomic-force microscopy (AFM) in an aqueous phase. The AFM image (Fig. S4A, ESI) shows the QDs are spherical with a mean height of 4.9 ± 0.52 nm from the corresponding height profile analysis (Fig.S4B, ESI†). The slightly different sizes measured by HAADF-STEM and AFM are presumably attributed to the β-LG layer.

Hydrodynamic diameter (D_h) is a key parameter for fluorescent probes used for *in vivo* imaging[30, 32]. Large probes (D_h >10 nm) typically accumulate in the liver while the small ones (D_h < 5 nm) undergo rapid renal excretion[30]. As shown in Fig. 1C, the average D_h of β-LG-Ag_2S QDs is determined as 5.7 ± 0.93 nm by dynamic light scattering (DLS). For this reason, the HD more accurately reflects the actual size of β-LG-Ag_2S QDs in the aqueous solution. The protein layer surrounding the Ag_2S core is approximately 0.7 ± 0.33 nm thick as shown in Fig. 1C (inset).

3.2. Photophysical Properties

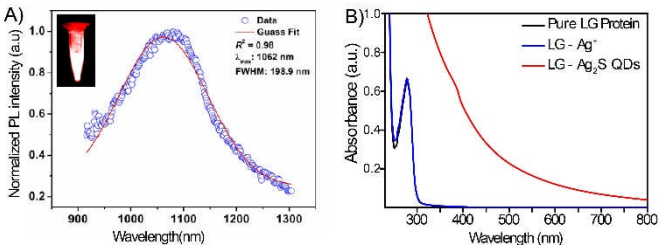

Fig. 2. (A) Photoluminescence (PL) spectrum of the freshly prepared β-LG-Ag_2S QDs. Inset: NIR-II fluorescence image of the QD solution excited at 808 nm. (B) UV-vis absorption spectra of β-LG, β-LG-Ag^+ complexes and β-LG-Ag_2S QDs.

Depending on the preparation method and surface coating, the emission of Ag_2S QDs can cover the visible, first and second near-infrared regions of the electromagnetic spectrum.[23, 33, 42-44] Compared to the visible/NIR-I QDs, NIR-II emitting Ag_2S QDs can provide deeper tissue penetration and significantly reduced tissue auto-fluorescence. The QD's PL spectrum of Fig. 2A shows a strong NIR-II fluorescence peaking at 1062 nm with a relatively narrow full-width-at-half-maximum (FWHM) of 199 nm (corresponding 0.22 eV), suggesting a relatively narrow size distribution. Notably, the emission spectra of NIR-II emitting Ag_2S QDs do not show clear size-dependent shift as reported in previous paper[45]. Moreover, the QY was calculated to be 5.68 % using the IR-26 dye as the reference standard (QY = 0.11%)[7, 46]. Fig. 2A (inset) shows a NIR-II fluorescence image of the β-LG-Ag_2S QD aqueous solution excited by an 808 nm laser light source. The QD suspension appears to be highly soluble and homogenous, presumably due to a large number of hydrophilic groups within the β-LG coating.

Fig. 2B shows the UV-vis absorption spectra of pure β-LG, β-LG-Ag^+ complexes (prepared by mixing β-LG and Ag^+ without the addition of Na_2S) and β-LG-Ag_2S QDs. Characteristic protein absorption is observed at ~280 nm for the β-LG and β-LG-Ag^+ complexes whereas the absorption of the β-LG-Ag_2S QDs is much broader and stronger, which also increases monotonously toward the shorter wavelength over the 250–800 nm range. The broad and greatly increased absorption is a typical indication of forming QDs[12].

The photophysical properties of the QDs can be highly sensitive to their surrounding environments if not well protected by surface coating, making quantitative fluorescence analysis difficult.[47, 48] Thus, effects of different environmental parameters (*e.g.*, pH, buffer, incubation time and temperature) on the PL intensity of β-LG-Ag_2S QDs were investigated. After 7-day incubation, the PL intensity showed little change or obvious shift of emission peak compared to the fresh samples at three different tested pH (5.4, 6.8, 7.4) and buffer conditions (Fig. S5 A-D, ESI†). Although β-LG is mostly dimeric at neutral pH, it dissociates into monomers at low pH and very low ionic strength condition because of intermolecular electrostatic repulsions[49, 50]. Previous studies showed that this protein can bind to more than one target molecule per monomer in acidic solution [51], which could enhance the stability of the complex under the acidic conditions of the stomach[39]. In this study, we attribute the robust photostability observed here to the effective protection of the β-LG coating [39, 41], which can isolate the Ag_2S cores from the environment.

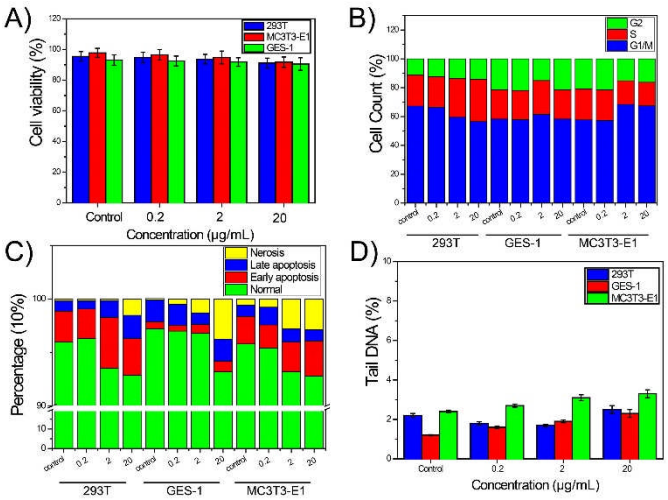

Fig. 3. *In vitro* cytotoxicity evaluation of the β-LG-Ag_2S QDs against human embryonic kidney (293T), human gastric epithelial (GES-1) and mouse fibroblast cell lines (MC3T3-E1). (A) Viability of 293T, GES-1 and MC3T3-E1 cells after incubation with 0.2, 2 and 20 μg/mL β-LG-Ag_2S QDs for 24 h; cells without treatment were used as the control. (B) Cell apoptosis analysis of 293T, GES-1 and MC3T3-E1 cells incubated with 0, 2 and 20 μg/mL β-LG-Ag_2S QDs for 24 h. (C) Histograms showing cell cycle phase distribution of 293T, GES-1 and MC3T3-E1 cells incubated with 0, 2 and 20 μg/mL β-LG-Ag_2S QDs for 24 h. (D) DNA damage levels (% tail DNA) evaluated in 293T, GES-1 and MC3T3-E1 cells exposed to 0.2, 2 and 20 μg/mL β-LG-Ag_2S QDs.

Although the PL gradually decreased with the increasing storage temperature compared to that stored at 4 °C (Fig. S5E&F, ESI†), possibly due to temperature-induced aggregation as observed in a similar system previously.[52] It is well known that thermal denaturation of β-LG at neutral and weakly basic pH is a complex, irreversible process[53] and involves the dissociation of β-LG dimer.[54] Simulated temperature dissociation profiles of β-LG show that the fraction of dissociated protein increases with increasing temperature from -15 to 85 °C[55]. One of the most important consequences of these conformational changes is the exposure of the free thiol (Cys121) in β-LG, which is highly reactive and can initiate the formation of intermolecular disulfide bonds [56, 57]. Disulfide-mediated aggregation is considered to be the key factor of thermotropic gelation of β-LG. In this work, the dissociation of β-LG increases with the increasing temperature from 4 to 37 °C, which may result in the aggregation of QDs, leading to decreased PL intensity after 7 days.

3.3. Biocompatibility of β-LG-Ag_2S QDs

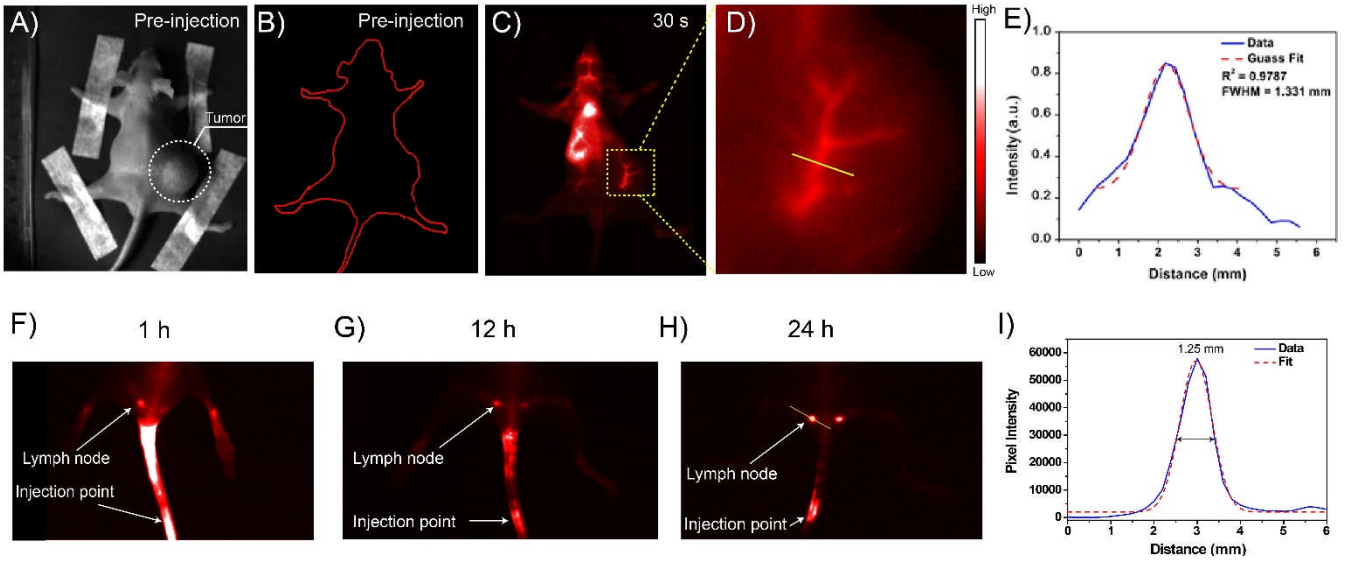

Fig. 4. *In vivo* NIR-II imaging of a tumor-bearing mouse with the β-LG-Ag_2S QDs. (A) Bright-field and (B) the corresponding NIR-II fluorescence images of a tumour-bearing mouse prior to QD injection. (C) NIR-II fluorescence image of the mouse at 30 s post-injection. (D) Zoomed-in NIR-II fluorescence image of the selected tumour area showing blood vessels. (E) Cross-sectional intensity profile along a yellow line shown in (D) with the peak fitted to a Gaussian function. The NIR-II fluorescence images of lymph node at (F) 1h, (G) 12 h and (H) 24 h after subcutaneous injection, respectively. (I) Cross-sectional intensity profile along a yellow line shown in (H) with the peak fitted to a Gaussian function.

The cytotoxicity of silver nanoparticles toward mammalian cells has been a concern, especially for those to be used for *in vivo* studies[58-60]. Therefore, the *in vitro* and *in vivo* toxicity of the QDs was further examined. First, the cytotoxicity of β-LG-Ag_2S QDs was evaluated using three cell lines: a human embryonic kidney cell line (293T), a human gastric epithelial cell line (GES-1) and a mouse calvaria-derived cell line (MC3T3-E1). Fig. 3A shows the viability of the cells after incubation with 0.2, 2 and 20 μg/mL of β-LG-Ag_2S QDs for 24 h No significant cell viability differences were observed between the QDs-treated and untreated control groups: more than 90% of the cells remained viable even at a relatively high QD concentration of 20 μg/mL, indicating that the QDs have negligible effects on cell proliferation for all three cell lines tested.

The effects of the QDs on cell apoptosis and cell cycle distribution were studied *via* flow cytometric analysis. Fig. 3B presents the percentage of 293T, GES-1 and MC3T3-E1 cells that were normal, necrotic, undergoing early apoptosis and undergoing late apoptosis after exposure to 2 and 20 μg/mL β-LG-Ag_2S QDs for 24 h against the untreated cell controls. The QDs did not induce significantly increased apoptosis. The population of normal cells did not decrease significantly after incubation with the β-LG-Ag_2S QD: >93% of cells in all three cell lines were found to be normal. Therefore, the QD did not have an adverse impact on cell cycle distribution (Fig. 3C). The QD-induced genotoxicity was further examined by determining the proportion of tail DNA in the QD-treated cells. Fig. 3D shows that the amount of tail DNAs induced by different concentrations of the β-LG-Ag_2S QD did not increase significantly in all three cell lines, indicating minimal genotoxicity of the QD. In fact, other groups have also confirmed the excellent biocompatibilities of both the Ag_2S QD and β-LG individually.[7,61-63] Given the fact that the β-LG-Ag_2S QDs are made of two biocompatible components, it is unsurprising that they show negligible cytotoxicity toward these cell lines. However, the potential immune response caused by β-LG cannot be neglected if the QDs are to be used clinically in the future, although this is beyond the scope of this paper.

3.4. *In vivo* Imaging of β-LG-Ag_2S QDs

Prior to QD injection, a bright-field (Fig. 4A) and the corresponding NIR-II fluorescence (Fig. 4B) images of the same tumor-bearing mouse revealed almost zero auto-fluorescence background in the NIR-II region. The *in vivo* imaging was carried out by injecting 200 μL of β-LG-Ag_2S QDs in PBS (pH=7.4) *via* the tail vein. The fluorescence signal was collected on a home-built NIR-II imaging system coupled with an InGaAs CCD camera. Fig. 4C shows that the fluorescence signals are detected throughout the mouse body at 30s post-injection. Fig. 4D presents well-defined vascular branches within the tumour area wherein the diameter of a blood vessel can be easily determined to be 1.33 mm *via* the cross-sectional intensity analysis (Fig. 4E). Fig. 4F to 4H show a time-course of NIR-II fluorescence images of mice after subcutaneous injection. Most of β-LG-Ag_2S QDs were blocked in the tail of mice, which could be distributed in the tissue fluid and enter the lymph node system via the microcirculation in the end. Specifically, the NIR-II fluorescence of the lymphatic area was weak at 1h post-injection but gradually migrated to the groin and become more intense over the following 24 h. Meanwhile, the fluorescence intensity around injection point correspondingly decrease due to the rapid metabolism of β-LG-Ag_2S QDs from body. Particularly, a lymph node within the region was visualized with a diameter of 1.25 mm (Fig. 4I). This result indicates that β-LG-Ag_2S QDs can be used as a useful NIR-II lymphatic tracer for *in vivo* lymph node imaging.

3.5. In Vivo Toxicity Evaluation of β-LG-Ag2S QDs

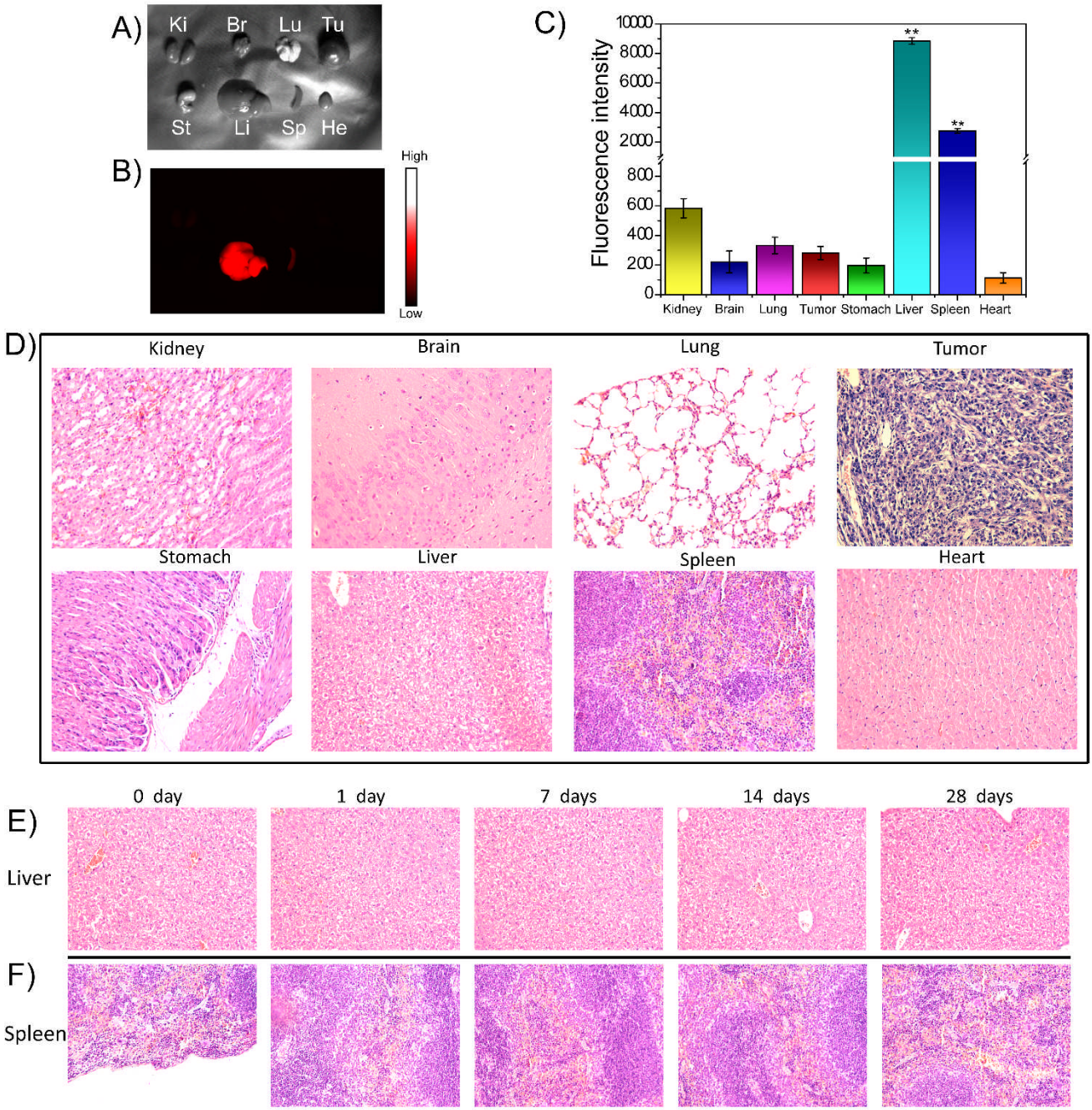

Fig. 5. (A) Bright-field and (B) corresponding fluorescence *ex vivo* images of major organs harvested from the tumor-bearing mice at 24 h post-injection. Ki, kidney; Br, brain; Lu, lung; Tu, tumor; St, stomach; Li, liver; Sp, spleen; H, heart. (C) Corresponding relative fluorescence intensities of the major organs. (D) H&E-staining images of the major organs including the kidney, brain, lung, tumor, stomach, liver, spleen and heart collected from the mice 24 h after β-LG-Ag_2S QD injection. Histological changes in the (E) liver and (F) spleen of the QDs-treated mice after injection with β-LG-Ag_2S QDs over a 28-day period. Original magnification, × 200 for D, E and F.

An *ex vivo* fluorescence analysis of the major organs (*i.e.* kidney, brain, lungs, stomach, liver, spleen and heart) and tumor harvested at 24 h post-injection revealed the accumulation of the QDs in the liver and spleen (Fig. 5 A & B). As shown in Fig. 5C, quantitative fluorescence analysis further verified this result: the liver and spleen exhibit higher fluorescence intensities than other major organs. This result is consistent with those reported in previous literature [28, 64].

Hematoxylin and eosin (H&E) staining was used to examine the potential toxic effect of β-LG-Ag_2S QDs on the major organs, *i.e.*, the kidney, brain, lung, tumor, stomach, liver, spleen and heart. The organs were harvested from the mice 24 h after injection of the QDs. As shown in Fig. 5D, significant lesions, inflammation patterns and other abnormalities caused by toxic nanomaterials were not observed in the organ tissues treated with the QDs. According to our *ex vivo* imaging results above, the QDs were accumulated mainly in

the spleen and liver. Therefore, a time-dependent H&E staining assay was conducted to monitor the possible long-term toxic effects of the QD toward these two organs. It is highly encouraging that no time-dependent damage or injuries to the spleens and livers of the QD-treated mice were observed over a 28-day experiment period (Fig. 5E and 5F).

4. Conclusions

To sum up, a NIR-II fluorescent Ag_2S QDs with excellent photo-stability and biocompatibility has been successfully prepared using β-LG as a bio-template. The strong NIR-II fluorescence together with excellent biocompatibility makes the QD an ideal fluorescent probe for *in vivo* imaging of small animals. Benefitted from the β-LG coating, the QDs are well dispersed in aqueous media with small hydrodynamic sizes. After intravenous injection, the QDs are rapidly spread throughout the mice's body, allowing for direct visualization of the capillary vessels around the tumors and lymph nodes. Such bright, biocompatible β-LG-Ag_2S QDs can be conjugated to targeting agents and/or therapeutic drugs to construct a multifunctional nano-platform which can be used for targeted imaging, drug delivery and therapeutic applications in the future.

Acknowledgements

We thank Dr Michael Ward (University of Leeds) for help in TEM imaging and Prof. Qiangbin Wang (Suzhou Institute of Nano-Tech and Nano-Bionics, Chinese Academy of Sciences, China) for help in the NIR-II imaging experiments. Y.K. thanks University of Leeds for providing a Fully-Funded International Research Scholarship (FFIRS) to support his study at Leeds. This project was supported by the University of Leeds (UK), Huashan hospital affiliated to Fudan University (China), the Royal Society-International Exchange Scheme (2014 and 2016 China NSFC costshare) and also in part by the National 863 Hi-tech Project (2015AA033703), the National Natural Science Foundation of China (Nos. 81271958, 81301672, 81401771, 81201773 and 81572108), the Natural Science Foundation of Shanghai Project (Nos. 12ZR1415800 and 15ZR1405000), the China Postdoctoral Science Foundation (No. 2014M560296) and the Innovation Program of the Shanghai Munivipal Education Commission (No.15ZZ006).

Author contributions

J.Chen, Y. Kong, Y. Wo and Y.Li designed the research; J.Chen, Y. Kong, H. Fang, Y. Dong, Y. Ge, Z. Wu, and T. Zhang performed the research; J. Chen and Y. Kong analyzed data; J. Chen, Y. Kong, S. Chen and D. Zhou wrote the paper. All authors have read, commented and approved the final version of the paper.

Notes and references

1. B. P. Thomas, E. B. Welch, B. D. Niederhauser, W. O. W. Jr, A. W. Anderson, J. C. Gore, M. J. Avison and J. L. Creasy, *J. Magn. Reson. Imaging*, 2008, **28**, 1266.
2. S. Diao, D. J. L. Blackburn, D. G. Hong, A. L. Antaris, J. Chang, J. Z. Wu, B. Zhang, K. Cheng, C. J. Kuo and H. Dai, *Angew. Chem. Int. Ed.*, 2015, **54**, 14758.
3. R. Weissleder and M. J. Pittet, *Nature*, 2008, **452**, 580.
4. R. G. Aswathy, Y. Yoshida, T. Maekawa and D. S. Kumar, *Anal. Bioanal. Chem.*, 2010, **397**, 1417.
5. A. M. Smith, M. C. Mancini and S. Nie, *Nat. Nanotech.*, 2009, **4**, 710.
6. J. O. Escobedo, O. Rusin, S. Lim and R. M. Strongin, *Curr. Opin. Chem. Biol.*, 2010, **14**, 64.
7. Y. Zhang, G. Hong, Y. Zhang, G. Chen, F. Li, H. Dai and Q. Wang, *ACS Nano*, 2012, **6**, 3695.
8. Z. Liu., C. Davis, W.B. Cai, L. He, X. Chen and H. Dai, *Proc. Natl. Acad. Sci. U. S. A.*, 2008, **105**, 1410.
9. K. W. Kevin, S. P. Sherlock and H. Dai, *Proc. Natl. Acad. Sci. U. S. A.*, 2011, **108**, 8943.
10. G. Hong, S. Diao, J. Chang, A. Antaris, C. Chen, B. Zhang, S. Zhao, D. Atochin, P. Huang, K. Andreasson, C.Kuo and H.Dai, *Nat. Photonics*, 2014, **8**, 723-730.
11. B. Dong, C. Li, G. Chen, Y. Zhang, Y. Zhang, M. Deng and Q. Wang, *Chem. Mater.*, 2013, **25**, 2503.
12. Y. Du, B. Xu, T. Fu, M. Cai, F. Li, Y. Zhang and Q. Wang, *J. Am. Chem. Soc.*, 2010, **132**, 1470.
13. Y. Guo, C. E. Rowland, R. D. Schaller and J. Vela, *ACS Nano*, 2014, **8**, 8334.
14. M.A. Langevin, A. M. Ritcey and C. N. Allen, *ACS Nano*, 2014, **8**, 3476.
15. A. Benayas, F. Ren, E. Carrasco, V. Marzal, B. del Rosal, B. A. Gonfa, Á. Juarranz, F. Sanz-Rodríguez, D. Jaque, J. García-Solé, D. Ma and F. Vetrone, *Adv. Funct. Mater.*, 2015, **25**, 6650.
16. J. Yang, Y. Hu, J. Tan, L. Jia, Y.-H. Zhu and J.-S. Yu, *J. Mater. Chem. B*, 2015, **3**, 6928.
17. F. C. J. M. van Veggel, *Chem. Mater.*, 2014, **26**, 111-122.
18. D. Naczynski, M. Tan, M. Zevon and B. Wall, *Nat. Commun.*, 2013, **4**, 1345.
19. N. Venkatachalam, T. Yamano, E. Hemmer, H. Hyodo, H. Kishimoto and K. Soga, *J. Am. Ceram. Soc.*, 2013, **96**, 2759.
20. I. Villa, A. Vedda, I. X. Cantarelli, M. Pedroni, F. Piccinelli, M. Bettinelli, A. Speghini, M. Quintanilla, F. Vetrone and U. Rocha, *Nano Res.*, 2015, **8**, 649-665.
21. G. Hong, Y. Zou, A. L. Antaris, S. Diao, D. Wu, K. Cheng, X. Zhang, C. Chen, B. Liu and Y. He, *Nat. Commun.*, 2014, **5**, 4206.
22. D. Ding, J. Liu, G. Feng, K. Li, Y. Hu and B. Liu, *Small*, 2013, **9**, 3093.
23. G. Hong, J. T. Robinson, Y. Zhang, D. Shuo, A. L. Antaris, Q. Wang and H. Dai., *Angew. Chem. Int. Ed.*, 2012, **51**, 9956.
24. C. Li, Y. Zhang, M. Wang, Y. Zhang, G. Chen, L. Li, D. Wu and Q. Wang, *Biomaterials*, 2014, **35**, 393.
25. F. Hu, C. Li, Y. Zhang, M. Wang, D. Wu and Q. Wang, *Nano Res.*, 2015, **8**, 1637.
26. G. Chen, F. Tian, Y. Zhang, Y. Zhang, C. Li and Q. Wang, *Adv. Funct. Mater.*, 2013, **24**, 2481-2488.
27. G. Chen, F. Tian, C. Li, Y. Zhang, Z. Weng, Y. Zhang, R. Peng and Q. Wang, *Biomaterials*, 2015, **53**, 265.
28. Y. Zhang, Y. Zhang, G. Hong, W. He, K. Zhou, K. Yang, F. Li, G. Chen, Z. Liu and H. Dai, *Biomaterials*, 2013, **34**, 3639.
29. H. S. Choi, W. Liu, F. Liu, K. Nasr, P. Misra, M. G. Bawendi and J. V. Frangioni, *Nat. Nanotech.*, 2010, **5**, 42.
30. H. S. Choi, W. Liu, P. Misra, E. Tanaka, J. P. Zimmer, I. B. Itty, M. G. Bawendi and F. Jv., *Nat. Biotech.*, 2007, **25**, 1165.

31. E. E. Lees, T.-L. Nguyen, A. H. A. Clayton and P. Mulvaney, *ACS Nano*, 2009, **3**, 1121.
32. T. Maldiney, C. Richard, J. Seguin, N. Wattier, M. Bessodes and D. Scherman, *ACS Nano*, 2011, **5**, 854.
33. R. G., J. Sun, D. Liu, Y. Wang and H. Jin, *Dalton Trans.*, 2014, **43**, 16690.
34. H. Yang, Y. Zhao, Z. Zhang, H. Xiong and S. Yu, *Nanotechnology*, 2013, **24**, 1.
35. G. Kontopidis, C. Holt and L. Sawyer, *J. Dairy Sci.*, 2004, **87**, 785.
36. W. Zhang and Q. Zhong, *Food Chem.*, 2010, **119**, 1318.
37. L. Liang, H. A. Tajmir-Riahi and M. Subirade, *Biomacromolecules*, 2008, **9**, 50.
38. J. K. Zimmerman, G. H. Barlow and I. M. Klotz, *Arch. Biochem. Biophys.*, 1970, **138**, 101.
39. S. Uhrínová, M. H. Smith, G. B. Jameson, D. Uhrín, L. Sawyer and P. N. Barlow, *Biochemistry*, 2000, **39**, 3565.
40. M. C. Yang, N. C. Chen, C. J. Chen, C. Y. Wu and S. J. T. Mao, *FEBS J.*, 2009, **276**, 2251.
41. M. Narayan and L. J. Berliner, *Biochemistry*, 1997, **36**, 1906.
42. H. Chen, B. Li, M. Zhang, K. Sun, Y. Wang, K. Peng, M. Ao, Y. Guo and Y. Gu, *Nanoscale*, 2014, **6**, 12580.
43. J. Peng, C. N. Zhu, Z. L. Zhang, Z. Q. Tian and D. W. Pang, *Biomaterials*, 2012, **33**, 5130.
44. C. N. Zhu, P. Jiang, Z. L. Zhang, D. L. Zhu, Z. Q. Tian and D. W. Pang, *ACS Appl. Mater. Interfaces*, 2013, **5**, 1186.
45. J. E. Murphy, M. C. Beard, A. G. Norman, S. P. Ahrenkiel, J. C. Johnson, P. Yu, O. I. Mic´ic, R. J. Ellingson and A. J. Nozik, J. Am. Chem. Soc., 2006, 128, 3241.
46. S. Tenzer, D. Docter, J. r. Kuharev, A. Musyanovych, V. Fetz, R. Hecht, F. Schlenk, D. Fischer, K. Kiouptsi and C. Reinhardt, *Nat. Nanotech.*, 2013, **8**, 772.
47. L. Martin, S. Johannes, E. Giuliano, L. Iseult, C. Tommy and D. Kenneth A, *Proc. Natl. Acad. Sci. U. S. A.*, 2008, **105**, 14265.
48. K. Sakurai, M. Oobatake and Y. Goto, *Protein Science : A Publication of the Protein Society*, 2001, **10**, 2325.
49. S. Kazumasa and G. Yuji, *J. Biol. Chem.*, 2002, **277**, 25735.
50. P. Zimet and Y. D. Livney, *Food Hydrocolloids*, 2009, **23**, 1120.
51. J. Chen, Y. Kong, J. Ji, J. Ruan, K. Wang, F. Gao and D. Cui, *Nanoscale*, 2012, **4**, 4455.
52. T. V. Burova, N. V. Grinberg, R. W. Visschers, V. Y. Grinberg and C. G. de Kruif, *Eur. J. Biochem.*, 2002, **269**, 3958.
53. M. J. Kelly and F. J. Reithel, *Biochemistry*, 1971, **10**, 3314.
54. R. K. Owusu Apenten and D. Galani, *Thermochim. Acta*, 2000, **359**, 181.
55. H. A. McKenzie and W. H. Sawyer, *Nature*, 1967, **214,**1101.
56. H. A. Mckenzie, G. B. Ralston and D. C. Shaw, *Biochemistry*, 1972, **11**, 4539.
57. P. V. Asharani, G. L. K. Mun, M. P. Hande and S. Valiyaveettil, *ACS Nano*, 2008, **3**, 279.
58. P. Chairuangkitti, S. Lawanprasert, S. Roytrakul, S. Aueviriyavit, D. Phummiratch, K. Kulthong, P. Chanvorachote and R. Maniratanachote, *Toxicol. In Vitro*, 2013, **27**, 330.
59. F. Sambale, S. Wagner, F. Stahl, R. R. Khaydarov, T. Scheper and D. Bahnemann, *J. Nanomater.*, 2015, **1,** 1.
60. T. Winuprasith, S. Chantarak, M. Suphantharika, L. He and D. J. Mcclements, *J. Colloid Interface Sci.*, 2014, **426**, 333.
61. X. Du, M. Zhiying, D. Zhang, F. Yuxin, M. Ma and Q. Chen, *Biosens. Bioelectron.*, 2014, **62**, 73.
62. X. Du, Z. Zhang, Z. Miao, M. Ma, Y. Zhang, C. Zhang, W. Wang, B. Han and Q. Chen, *Talanta*, 2015, **144**, 823.
63. L. Balogh and N. B. M. Nair, *Nanomedicine (New York, NY, United States)*, 2007, **3**, 281.

